J. Appl. Comput. Mech., xx(x) (2026) 1-14
DOI: 10.22055/jacm.2026.48778.5490

ISSN: 2383-4536
jacm.scu.ac.ir

Shahid Chamran University of Ahvaz

Journal of Applied and Computational Mechanics

Research Paper

Numerical Investigation of a Concentrating Photovoltaic Cooling System Using a Heat Sink with Nanoparticle-Enhanced Phase Change Materials

Ramin Vatandoust[1], Arash Mirabdolah Lavasani[1], Saeed Dinarvand[1], Mohamad Eftekhari Yazdi[1], Mohammad Sardarabadi[2]

[1] Department of Mechanical Engineering, CT.C., Islamic Azad University, Tehran, Iran

[2] Department of Energy Engineering, Faculty of Advanced Technologies, Quchan University of Technology, Quchan, Iran

Received September 22 2025; Revised May 17 2026; Accepted for publication May 17 2026.
✉ Corresponding author: A. Mirabdolah Lavasani (arashlavasani@iau.ac.ir)

Abstract. In this study, the cooling of a Concentrator Photovoltaic (CPV) system with a heat sink is investigated numerically. For this purpose, a two-dimensional model including the CPV cell, phase change material, and 3% and 5% CuO nanoparticles is developed. The 2D numerical simulation is based on the enthalpy method. Validation is performed based on available experimental data. The validation shows that the difference is around 2%; therefore, the simulation is acceptable. Results show that using 5% CuO nanoparticles instead of 3% CuO nanoparticles or pure PCM increases the heat transfer coefficient and lowers the CPV solar cell temperature, ultimately boosting system efficiency. The best results are achieved with 5% CuO, reducing the panel's temperature by up to 11°C compared to pure PCM. This leads to a noticeable improvement in electrical efficiency, increasing it from 2.55% with pure PCM to 3.37% with 5% CuO.

Keywords: Nanoparticles, Phase Change Materials (PCM), Nanoparticle-Enhanced Phase Change Materials (NEPCM), Concentrating Photovoltaic Panels (CPV); Heat Sink.

1. Introduction

Concentrator Photovoltaic (CPV) panels are gaining attention for their many advantages, including higher electrical efficiency, lower investment costs per watt, and applications in advanced electronics and space technology. These systems can achieve 25% to 30% greater efficiency than conventional photovoltaic panels by focusing sunlight onto a smaller area using Fresnel lenses, parabolic mirrors, or reflectors. These optical elements capture solar irradiance over a larger surface and concentrate it onto high-efficiency solar cells [1]. However, one of the biggest challenges in CPV technology is heat buildup. In silicon-based photovoltaic systems, only about 18–20% of the incoming solar energy is converted into electricity, while the rest turns into heat [2]. This excess heat increases the temperature of the solar cells, reducing their efficiency. In monocrystalline and polycrystalline silicon solar cells, a higher temperature slightly increases the short-circuit current (by 0.06–0.1% per °C) but significantly decreases the output voltage (by 2–2.3 mV per °C) and fill factor (by 0.1–0.2% per °C). As a result, electrical power output declines by approximately 0.4–0.5% per °C [3-5].

Due to the use of silicon-based solar cells in the structure of concentrator panels, the problem of increasing cell temperature and decreasing efficiency was also observed in these systems Concentrating panels are divided into three general categories based on the degree of concentration ratios (CR). In panels with a low degree of concentration ratios (between 2 and 10), cooling and moving equipment (to rotate the panel in the direction of the sun) was not needed, unlike this case, in the type of concentrator with a medium ratios and high degree of concentration ratios (between 10 and 1000), in addition to the need for a mover, the need to use passive and active methods to cool the panel is one of the most important factors required [5]. One of the most effective ways to cool photovoltaic panels is by using a heat sink (HS). When combined with phase change materials (PCMs) and nanoparticles, this approach significantly enhances heat transfer, reducing the operating temperature of solar cells and ultimately improving electrical efficiency [6]. Several studies have explored different cooling methods for photovoltaic systems, particularly focusing on the integration of PCMs and nanoparticles.

Khodadadi et al. [7] investigated the use of aluminum oxide nanoparticles in a photovoltaic system with a Fresnel reflector, analyzing the impact of different mass flow rates. They found that while adding nanoparticles at low mass flow rates reduced

Published online: May 21 2026

electrical efficiency, the overall combination of PCMs and nanoparticles improved heat transfer and system performance. Similarly, Kothari et al. [8] studied the effect of nanoparticles in a heat exchanger, with and without fins, and observed that lower aluminum oxide nanoparticle concentrations (0–6%) achieved the highest heat transfer efficiency. In another study, Aqib et al. [9] experimentally examined the impact of aluminum oxide nanoparticles and carbon nanotubes on PCM cooling performance. Their findings showed that combining paraffin with these nanoparticles significantly enhanced heat transfer compared to using pure PCM. Ismail et al. [10] further analyzed a heat sink for cooling CPV panels, comparing the effectiveness of aluminum oxide, copper oxide, and silicon oxide nanoparticles in PCMs against non-nanoparticle PCMs. Their results highlighted the superior cooling performance of nanoparticle-enhanced PCMs.

Research on CPV cooling has also focused on optimizing heat sink designs. Imam et al. [11] explored four different configurations, single cavity, three parallel cavities, five parallel cavities, and three series cavities, demonstrating that designs with more parallel cavities enhanced thermal efficiency, reduced cell temperature, and improved CPV electrical performance. Najafi et al. [12] examined a mini-channel heat sink with nano-PCMs for electronic chip cooling, concluding that adding nanoparticles significantly boosted heat exchange efficiency. Esmail et al. [13], analyzed the impact of sintered porous media microchannel heat sinks for thermal management of CPVs. Based on their results, cell temperature reduced by 15.3%, 8.97%, and 2% at concentration ratios of 20000, 10000, and 2000, respectively. Radwan et al. [14] simulated a CPV cooling heat sink under various conditions, including concentration ratios of 20–40%, mass flow rate of 100 Reynolds, wind speed variations, and different inlet fluid temperatures. Their results indicated that increasing both the concentration ratio and mass flow rate led to better heat transfer and improved power output. In a follow-up study, Radwan et al. [15], investigated a microchannel heat sink with nanofluids, using aluminum oxide and silicon carbide nanoparticles as PV coolants.

Hovank et al. [16], also explored CPV cooling using a porous medium heat sink with PCMs, finding that greater material height and porosity maximized electrical output. Lamba et al. [17] have shown that integrating phase change materials (PCMs) with passive cooling techniques such as heat sinks and radiative cooling can significantly enhance photovoltaic thermal regulation due to the high latent heat storage capacity of PCMs. Numerical investigations using multiphysics models have shown that hybrid configurations can significantly reduce PV operating temperatures and improve power output under high solar radiation and harsh weather conditions. In another study, Po et al. [18] investigated the thermal management of photovoltaic cells using PCM-based heat sinks with different T-shaped fin configurations using COMSOL Multiphysics software. The results showed that an optimized 180° T-shaped fin significantly improved temperature uniformity, reduced the PV cell temperature by 15.1 K, and increased the electrical efficiency by about 1.4%, highlighting the critical role of fin geometry in PCM-based PV cooling systems. In a separate work, Rao et al. [19] investigated the use of a conventional PCM (HS36) and a graphene-based nano-enhanced PCM (NePCM) for photovoltaic thermal management.

The addition of 0.9 wt.% graphene flakes improved the PCM's thermal conductivity by 47% and reduced the PV cell temperature by nearly 10 °C, resulting in over 12% higher electrical efficiency—highlighting the effectiveness of graphene additives for augmenting PCM heat transfer in solar applications. In a closely related work, Alipour et al. [20] numerically analyzed a concentrating photovoltaic (CPV) cooling system incorporating a heat sink filled with nanoparticle-enhanced phase change materials (NEPCM).

Using CuO nanoparticles at 3 wt.% and 5 wt.% within n-octadecane, they observed that the 5 wt.% composition achieved the most effective heat transfer enhancement—reducing the CPV cell temperature by up to 11 °C and raising electrical efficiency from 2.55 % to 3.37 %. The findings confirm that increasing nanoparticle concentration intensifies natural convection and accelerates melting, leading to better thermal regulation and higher electrical performance of CPV modules.

In another research, Lima-Téllez et al. [21] numerically investigated a 3D photovoltaic thermal (PVT) system integrated with phase change material and copper metal foam using a nanofluid as the working fluid. The results showed that increasing metal foam porosity significantly enhanced thermal efficiency (up to 33%), while the incorporation of copper foam improved both thermal and electrical efficiencies compared to the conventional PVT/PCM configuration. In a related work, Becheikh et al. [22] numerically examined the thermal and electrical performance of photovoltaic panels cooled by different nanofluids (Al_2O_3, CuO, and ZnO) flowing through a novel parallel channel equipped with baffles. The results indicated that CuO nanofluid provided the highest thermal efficiency improvement (up to 5.67%), while the combined use of nanoparticles and baffles enhanced heat transfer and increased electrical efficiency by up to 4% under low Reynolds numbers.

In another study, Togun et al. [23] investigated the transient thermal behavior of a photovoltaic panel cooled by a paraffin-based phase change material enhanced with internal fins and Cu nanoparticles using an implicit numerical scheme. Beyond thermal performance, the study assessed environmental and economic impacts, showing that nanoparticle incorporation improved heat transfer, increased profitability by up to 2.75% after 90 min, and enhanced CO_2 mitigation by approximately 1.27%, although long-term operation led to reduced profitability, particularly in finned configurations.

Gholami et al. [24] experimentally and numerically investigated fin enhanced phase change material heat sinks for photovoltaic cooling. The results showed that optimized fin configurations significantly reduced PV operating temperature and improved electrical efficiency, particularly during peak solar irradiation periods. Hasan et al. [25] examined the effect of metal oxide and carbon-based nanoparticles on the thermal behavior of PCM based PV cooling systems. Their findings demonstrated faster melting rates and improved heat dissipation, leading to enhanced temperature stability of the photovoltaic module.

Despite extensive research on cooling techniques for Concentrator Photovoltaic (CPV) systems, significant gaps remain in optimizing thermal management strategies. While several studies have investigated the use of phase change materials (PCMs) and nanoparticle-enhanced PCMs (NEPCMs) for heat dissipation, they often focus on specific nanoparticles such as aluminum oxide (Al_2O_3) or silicon carbide (SiC), with limited attention given to copper oxide (CuO) despite its promising thermal properties. Additionally, many studies have primarily examined cooling strategies for low-concentration CPV systems, leaving medium- to high-concentration ratio (CR) panels underexplored. The impact of various heat sink geometries has been analyzed, yet a comprehensive approach that integrates heat sinks with NEPCMs to maximize cooling efficiency is still lacking. Furthermore, previous research has not fully addressed the trade-off between increased thermal conductivity and potential sedimentation issues at higher nanoparticle concentrations, which can reduce heat transfer performance. The accuracy of numerical simulations also varies, with many studies relying on simplified models that lack experimental validation.

To address these gaps, this study introduces an innovative cooling approach by integrating a heat sink with CuO nanoparticle-enhanced PCM (NEPCM), leveraging both passive and enhanced thermal management strategies. A two-dimensional numerical model is developed using the enthalpy-porosity method in ANSYS FLUENT, ensuring a highly accurate representation of the heat transfer process. This research aims to provide new insights into optimizing CPV cooling technologies, contributing to the development of more efficient and sustainable photovoltaic systems.

2. Theoretical Analysis

2.1. Geometry

The selected geometry of the CPV system in this project is shown in Fig. 1. This system consists of two coupled components: a photovoltaic module and a PCM enclosure. The photovoltaic module comprises a 2 mm thick glass layer and a 0.5 mm thick silicon cell layer, designed to efficiently capture and convert concentrated sunlight into electricity. To regulate the module's temperature, a rectangular PCM enclosure is placed in direct contact with the module. This enclosure measures 125 mm in height and 100 mm in length and is filled with a nanoparticle-enhanced phase change material (NEPCM) to improve heat dissipation. The system operates under a solar concentration ratio (CR) of 20, meaning that the solar energy focused onto the module is 20 times the standard 1,000 W/m^2 irradiance. Further details regarding material properties and system specifications are provided in Tables 1 and 2.

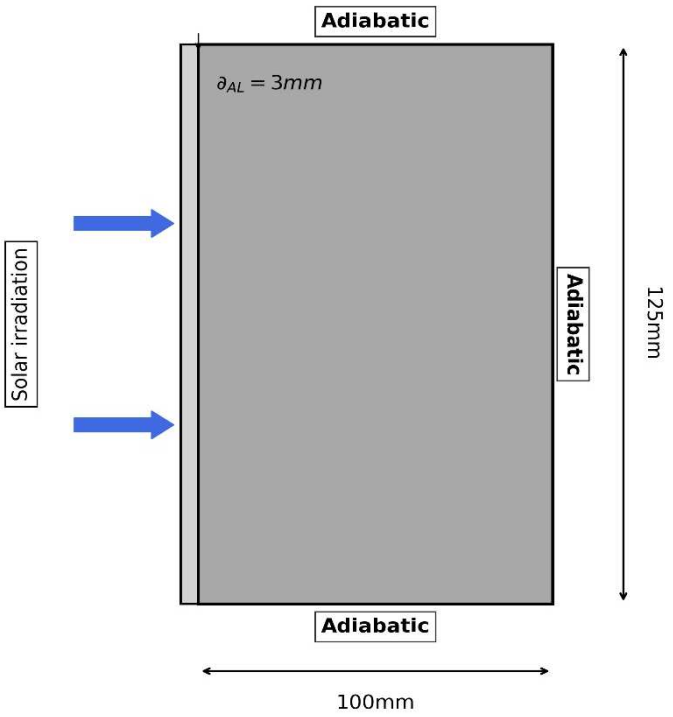

Fig. 1. The geometry of the CPV.

Table 1. Optical and Thermophysical Properties of the Materials Used in the PV Module.

Thermo-physical properties	Glass	EVA	CELL	Aluminum
Thickness (mm)	3	0.5	0.2	3
Spec. heat cap. (kJ/kg K)	500	2070	677	0.903
Density (kg/m^3)	3000	960	2330	2675
Thermal cond. (W/mK)	2	0.35	148	211

Table 2. The thermophysical properties of the PCM and nanoparticles [10].

Thermo-physical properties	PCM n-octadecane	Aluminum (Al)	Copper Oxide (CuO)
Thermal cond. (W/mK) Solid/ Liquid	0.358 0.148	211	18
Density (kg/m^3) Solid/ Liquid	865 770	2675	6510
Spec. heat cap. (kJ/kg K) Solid/ Liquid	1934 2196	0.903	540
Melting point (°C)	28oc	-	-
Heat of fusion (kJ/kgK)	243	-	-
Thermal exp. coefficient (l/k)	0.00091	-	0.0000167
Diameter (nm)	-	-	29

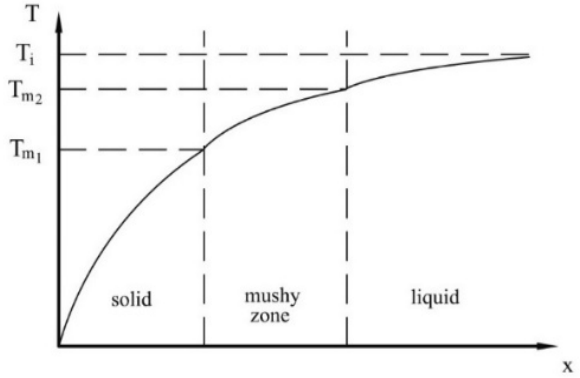

Fig. 2. Phase change volume with mushy porous zone.

2.2. Governing equations

2.2.1. *Assumptions*

This study is based on the following assumptions:

- The heat sink's geometric dimensions remain constant throughout the analysis and all sidewalls are considered adiabatic.
- The melting process is unsteady and fluid flow is laminar and two-dimensional.
- The melted PCM-nanoparticle composite is incompressible and Newtonian.
- The mass flow rate, ambient temperature, and total volume of both the PCM and nanoparticles are assumed to remain constant.
- The NEPCM is assumed to be homogeneous.
- The thermophysical properties of the PV layers, PCM, nanoparticles, and aluminum in the solid phase are treated as isotropic and temperature-independent.
- Thermophysical properties of the PCM and, nanoparticles in the liquid phase are temperature-dependent.

2.2.2. *Concentrate photovoltaic (CPV)*

Due to the inclusion of an aluminum layer in contact with the CPV, the heat transfer diffusion equation is applied in Cartesian coordinates [26, 27]:

$$\nabla \cdot (\mathrm{k}_i . \nabla \mathrm{T}_i) + \ q_i = \rho_i \ . C_{p,i} . \frac{\partial t_i}{\partial \mathrm{T}} \qquad \text{for i} = 1,2,... \tag{1}$$

In this equation, $\mathrm{T}_i(x,y)$ represents the temperature, $C_{p,i}$, ρ_i, q_i and k_i are the specific heat, density, interior heat generation and thermal conductivity of the layer i, respectively. Also, the heat generation per unit volume of the layer i, is as follows [11, 28]:

$$q_i = \frac{(1-\eta_{sc})\ G(t)\ \alpha_i\ \tau_i\ A_i}{V_i} \tag{2}$$

where η_{sc} is the electrical efficiency of the silicon layer in the solar cells, $G(t)$ is the solar concentrated irradiance, α_i, V_i, A_i and τ_i are absorptivity, volume, area, and transmissivity of the layer i, respectively. Finally, the following equation is used to calculate the electrical power of the PV [10, 11, 29]:

$$P_{pelec} = \eta_{Sc} \ . G(t) . H_1 . S_c . \tau_g . E \tag{3}$$

where G is considered 1000 W/m^2 (standard irradiation value), H_1 is the height of the PV, and η_{Sc} is the efficiency of the PV that can be obtained by the following equation:

$$\eta_{Sc} = \eta_{ref}\ (1 - \beta_{ref}(T_{SC} - \ T_{ref}\ ) \tag{4}$$

2.3. Nanoparticles-enhanced phase change materials (NEPCM)

The enthalpy-porosity method is used in this study to analyze phase changes within the PCM-nanoparticle composition. As described by Voller [30], this approach models the mushy region, the transitional phase between solid and liquid, as a porous medium (see Fig. 2). In this model, the porosity of each computational cell corresponds to the local liquid fraction, allowing for a more accurate representation of phase change dynamics. In fully solidified regions, the porosity is set to zero, effectively restricting fluid motion and ensuring realistic velocity behavior. The governing equations for the enthalpy-porosity method are as follows:

2.3.1. *Continuity*

The continuity equation can be described as:

$$\frac{\partial u}{\partial x} + \frac{\partial v}{\partial y} = 0 \tag{5}$$

2.3.2. *Momentum*

Momentum in X and Y directions can be expressed as:
- X-direction:

$$\rho_{\mathrm{l,npcm}} \cdot \frac{\partial \mathrm{u}}{\partial \mathrm{t}} + \rho_{\mathrm{l,npcm}} \cdot u \ \frac{\partial \mathrm{u}}{\partial \mathrm{x}} + \rho_{\mathrm{l,npcm}} \cdot v \ \frac{\partial \mathrm{u}}{\partial \mathrm{y}} = \ - \ \frac{\partial \mathrm{P}}{\partial \mathrm{x}} + \mu_{\ \mathrm{l,npcm}} \ (\frac{\partial^2 \mathrm{u}}{\partial \mathrm{x}^2} + \frac{\partial^2 \mathrm{u}}{\partial \mathrm{y}^2}) + \ S_x \tag{6}$$

- Y-direction:

$$\rho_{\mathrm{l,npcm}} \cdot \frac{\partial \mathrm{v}}{\partial \mathrm{t}} + \rho_{\mathrm{l,npcm}} \cdot u \frac{\partial \mathrm{v}}{\partial \mathrm{x}} + \rho_{\mathrm{l,npcm}} \cdot v \frac{\partial \mathrm{v}}{\partial \mathrm{y}} = -\frac{\partial \mathrm{P}}{\partial \mathrm{Y}} + \mu_{\mathrm{l,npcm}} \left(\frac{\partial^2 \mathrm{v}}{\partial \mathrm{x}^2} + \frac{\partial^2 \mathrm{v}}{\partial \mathrm{y}^2}\right) + S_y + F_B \tag{7}$$

where S_x and S_y are Darcy's law added to momentum equations due to the phase change effect on convection:

$$S_x = \frac{(1-\lambda)^2}{(\lambda^3+\gamma)} \cdot A_{Mush} \cdot u \tag{8}$$

$$S_y = \frac{(1-\lambda)^2}{(\lambda^3+\gamma)} \cdot A_{Mush} \cdot v \tag{9}$$

where λ is the liquid volume fraction, γ is a small number (0.001) to prevent division by zero, A_{Mush} is the mushy zone constant, when this value is high, it shows transition of the material velocity to zero when the material solidifies [31]. The mushy zone constant (A_{Mush}) is typically recommended to be around 10^4 to 10^7. The most commonly used value is 10^6, as it provides a good balance between numerical stability and physical accuracy when modeling phase change processes using the enthalpy-porosity method. Therefore, the amount of A_{Mush} is considered to be 10^6 [26, 27, 32].

2.3.3. *Energy equation*

Some experimental and numerical researches have performed to evaluate the heat transfer with solid-liquid PCMs. In the present article, the Enthalpy methods $(H-P)$ is used to analyze the results [33].

2.3.3.1. *Enthalpy method*

Generally, the enthalpy of the material is computed as the sum of the sensible enthalpy, h, and the latent heat $\Delta\mathrm{H}$:

$$H = h_1 + \Delta\mathrm{H} \tag{10}$$

$$h_1 = h_{ref} + \int_{T_{ref}}^{T} C_P . \mathrm{dT} \tag{11}$$

h_{ref} = reference enthalpy
T_{ref} = reference temperature
C_P = specific heat at constant pressure

The latent heat term now can be written of the latent heat for Nanoparticles PCM:

$$\Delta\mathrm{H} = \lambda . \mathrm{L} \tag{12}$$

The liquid fraction, λ, can be defined as:

$$\lambda = 0 \quad \text{if} \quad \mathrm{T} < T_{solid}$$
$$\lambda = 1 \quad \text{if} \quad \mathrm{T} > T_{solid}$$
$$\lambda = \frac{(\mathrm{T} - T_{Solid})}{(T_{Liquid} - T_{Solid})} \quad \text{if} \quad T_{Solid} < \mathrm{T} < T_{solid}$$

The latent heat content $\Delta\mathrm{H}$, can vary between zero (for the solid state) and 1 (for the liquid). For solidification/melting process, the energy equation is written as:

$$\frac{\partial(\rho\mathrm{H})}{\partial \mathrm{t}} + \nabla . (\rho . \mathrm{v} . \mathrm{H}) = \nabla . (\mathrm{k} . \nabla . \mathrm{T}) + \mathrm{S} \tag{13}$$

where H, ρ, v, S are enthalpy, density, fluid velocity, and source term, respectively. Here the definition of the heat source term is [31, 34]:

$$S = \rho . \frac{\partial \Delta H}{\partial \mathrm{t}} \tag{14}$$

In general, within the PCM/nanoparticle composition, nanomaterials influence the thermophysical properties of the PCM. These properties, including density, heat capacity, and the heat transfer coefficient depend on the volume fraction of the nanoparticles. The following equation is used to convert between mass and volume fractions ($\emptyset wt$ to $\emptyset$) [35]:

$$\emptyset = \frac{\emptyset wt \ . \ \rho_{\mathrm{pcm}}}{\emptyset wt \ . \rho_{\mathrm{pcm}} + (1 - \emptyset wt) . \rho_{\mathrm{p}}} \tag{15}$$

Density of the PCM/nano particle can be described as:

$$\rho_{\mathrm{npcm}} = (1-\emptyset)\rho_{\mathrm{pcm}} + \emptyset\rho_{\mathrm{p}} \tag{16}$$

$$\rho_{\mathrm{pcm}} = \begin{cases} \rho s & T < Tm \\ \dfrac{(\rho s + \rho l)}{2} & Tm < T < Tm + \Delta Tm \\ \rho l & T \geq Tm + \Delta Tm \end{cases} \tag{17}$$

where Tm is the melting temperature of the PCM, and ΔTm is the phase transition temperature range, difference among the liquids and solid temperatures, which is defined as:

$$\Delta Tm = T_{Liquids} - T_{solids} \tag{18}$$

The heat capacity of the PCM/nanoparticles composition and part of the Boussinesq term as represented below:

$$(\rho. C_p)_{npcm} = (1 - \emptyset)(\rho C_p)_{pcm} + \emptyset(\rho. Cp)_p \tag{19}$$

$$(\rho. \beta)_{npcm} = (1 - \emptyset)(\rho. \beta)_{pcm} + \emptyset(\rho. \beta)_p \tag{20}$$

The latent heat is defined as:

$$(\rho. \lambda\ )_{npcm} = (1 - \emptyset)(\rho. \lambda)_{pcm} \tag{21}$$

The modified heat capacity of the PCM is formulated as follows:

$$(\rho Cp)pcm \quad = \begin{bmatrix} (\rho Cp)s & T < Tm \\ \dfrac{(\rho Cp)s + (\rho Cp)l}{2} + \dfrac{\rho s + \rho l}{2}\left(\dfrac{\lambda}{\Delta Tm}\right) & Tm < T < Tm + \Delta Tm \\ (\rho Cp)l & T \geq Tm + \Delta Tm \end{bmatrix} \tag{22}$$

The viscosity of the colloid containing weak suspensions of the small rigid sphere-shaped particles viscosity is defined by Brinkman [36]:

$$\mu = \frac{\mu l}{(1 - \emptyset)^{2.5}} \tag{23}$$

The effective thermal conductivity (K_o) of the PCM /nanoparticles composition is defined by the model of Maxwell as follows [35]:

$$\frac{Knpcm}{Kpcm} = \frac{Kp + 2Kpcm - 2\emptyset(Kpcm - Kp)}{Kp + 2Kpcm + \emptyset(Kpcm - Kp)} \tag{24}$$

$$Kpcm = \begin{bmatrix} Ks & T < Tm \\ \dfrac{(Ks + Kl)}{2} & Tm < T < Tm + \Delta Tm \\ Kl & T \geq Tm + \Delta Tm \end{bmatrix} \tag{25}$$

Thermal conductivity improvement due to thermal diffusion is:

$$Kd = b.(\rho. Cp)n\sqrt{u^2 + v^2}. \emptyset d_p \tag{26}$$

Note that, the empirically-determined constant b is estimated by Wakao and Kaguei [37]. Therefore, the effective thermal conductivity of the colloid is defined by:

$$K_n = K_o + K_d \tag{27}$$

2.4. Boundary conditions

The boundary conditions, which was shown in Fig. 1, are as follows:

A. The boundary condition of non-slip is applied in the area between the solid-liquid phases:

$$x = \delta_{\mathrm{Al}},\ (\mathrm{L} - \delta_{\mathrm{Al}}):\ \ y = 0,\quad \mathrm{H1}\quad for\ \ t \geq 0$$

$$x = \delta_{\mathrm{Al}}: y = 0,\quad for\ t \geq 0$$

B. The initial conditions are equal to:

$$u(x, y, z) = u(x, y, 0) = 0 \tag{28}$$

C. The ambient temperature is considered to be 25°C

D. The boundary conditions of the CPV inlet wall are a combination of heat transfer - convection and radiation:

$$-k\frac{\partial T}{\partial \mathrm{X}} = h_{conv\ ,\mathrm{g-amb}}(T_{amb} - T_g) + h_{\mathrm{rad}\ ,\mathrm{g-sky}}(T_{sky} - T_g) \tag{29}$$

E. Boundary conditions of the wall between the CPV system and the box:

$$-k\frac{\partial T}{\partial \mathrm{X}} = \ h_{conv}(\ T_{amb} - \ T_{al}) \tag{30}$$

F. In Eq. (31), the values of displacement and radiation heat transfer coefficients are defined as follows:

$$h_{\mathrm{rad}\ ,\mathrm{g-sky}} = \sigma.\varepsilon.g\frac{(T_g^4 \quad - T_{sky}^4)}{(T_g - T_{sky})} \tag{31}$$

$$h_{conv\ ,\mathrm{g-amb}} = 5.7 + 3.8V_m \tag{32}$$

G. In Eq. (32), the wind speed V_m is considered equal to 1 m/s.

H. The top, bottom and end walls are considered adiabatic:

$$-k\frac{\partial T}{\partial \mathrm{X}} = 0 \tag{33}$$

3. Numerical Solution

In this study, numerical modeling is conducted using ANSYS FLUENT 19.0 software, to simulate the thermal behavior of the system. The following settings and assumptions are applied in the software:

- Pressure-based solver with transient flow is selected to capture time-dependent variations.
- Energy and solidification & melting models are activated to account for phase change phenomena.
- The SIMPLE algorithm is used for pressure-velocity coupling to ensure computational stability.
- A second-order upwind scheme is applied for both momentum and energy equations, enhancing accuracy in numerical calculations.

3.1. Grid independency

To ensure the grid independence of the proposed numerical model, four different computational grids (A to D) were employed. The characteristics of these grids, including the number and size of elements, are summarized in Table 3. The grid refinement was performed by increasing the total number of nodes from 82,267 to 185,903 and reducing the element size from 0.4 to 0.25.

Initially, grid independence was evaluated based on the liquid fraction variable. The results indicate that increasing the grid resolution leads to a decrease in the liquid fraction from 0.041 to 0.034, while no significant variation is observed between the finer grids (C and D). This behavior confirms that the numerical solution becomes insensitive to further mesh refinement, validating the selection of Grid C as an appropriate grid from the standpoint of phase change prediction.

In addition to the liquid fraction, the average solar cell surface temperature (Tsc) was further employed as a key thermal parameter to assess grid independence. The parameter Tsc was defined as the area-averaged temperature of the solar cell surface and was evaluated at the final simulation time (t = 80 min). This time was selected as a reference because the system reaches a quasi-steady thermal state, where the influence of initial transient effects is significantly reduced. It should be noted that this time does not correspond to the complete melting of the phase change material, but rather represents a suitable reference time for numerical convergence analysis.

The grid independence results based on Tsc show that increasing the number of nodes leads to progressively smaller variations in the average solar cell temperature. In particular, the relative difference in Tsc between the two finest grids (C and D) is less than 0.1%, demonstrating satisfactory convergence and confirming the grid-independent nature of the numerical results.

Based on the combined analysis of both liquid fraction and average solar cell temperature, grid C was selected for all subsequent simulations, as it provides an optimal balance between numerical accuracy and computational efficiency. The time step for the calculations was set to 0.1 s, and convergence was verified at each time step using a convergence criterion of 10^{-6} for all solution variables.

A schematic view of the utilized grid is depicted in Fig. 3. In addition to the grid independence analysis, the quality of the selected computational mesh (grid C) was carefully evaluated to ensure numerical accuracy and stability. Figure 3 illustrates the structure of the utilized grid, while the corresponding mesh quality parameters are summarized in Table 4.

The average skewness value of the mesh is 0.027, with a maximum value of 0.515, which lies well within the acceptable range recommended by ANSYS (0–0.5 for good-quality meshes). This indicates a highly uniform and well-shaped grid with negligible distortion. Moreover, the orthogonal quality exhibits an average value of 0.9998 and a minimum value of 0.817, both of which are very close to the ideal value of unity.

These results confirm that the selected mesh (grid C) possesses excellent quality and is suitable for accurately capturing the thermal and fluid flow behavior of the CPV/PCM system without introducing numerical errors associated with poor mesh quality.

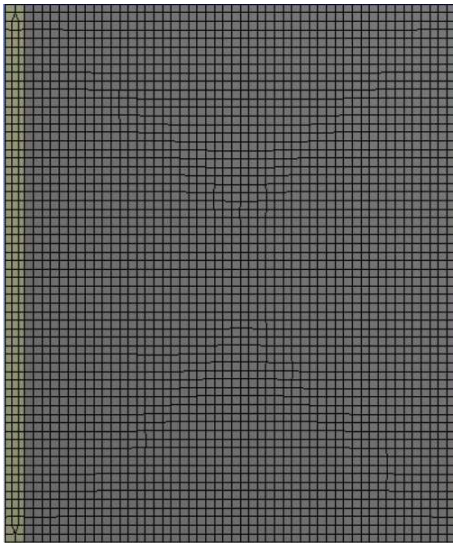

Fig. 3. View of the utilized grid.

Table 3. Grid dependence of the numerical solution.

Different networks	Number of nodes	Element size	Liquid fraction	Average solar cell temperature, Tsc (°C)
A	82267	0.4	0.041	191.4
B	145189	0.31	0.035	188.9
C	166455	0.28	0.034	188.2
D	185903	0.25	0.034	188.1

Table 4. Mesh quality parameters of the selected grid (grid C).

Mesh quality parameter	Average	Minimum	Maximum	Acceptable range of ANSYS
Skewness	0.027	1.3×10^{-5}	0.515	0 -0.5 (Good Range)
Orthogonal Quality	0.9998	0.817	1	Numbers close to 1 (Good Range)

Table 5. Thermophysical properties of PCM-CuO nanomaterial Composites at 3 wt % and 5 wt%.

Thermophysical properties	n-octadecane-CuO 5%	n-octadecane-CuO 3%
Thermal cond. (W/mK) Solid/Liquid	0.359	0.358
Density (kg/m^3) Solid/Liquid	870.1	868.14
Spec. heat cap. (kJ/kg K) Solid/Liquid	1924.6	1928.18

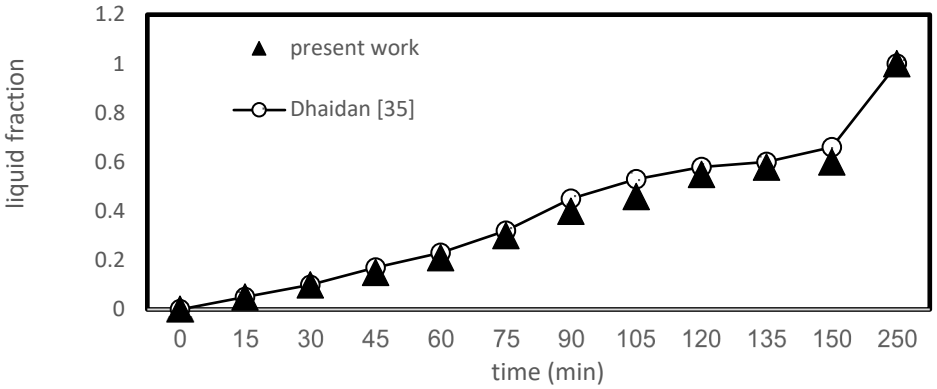

Fig. 4. Comparison between Dhaidan et al. [35], and the results of the present study on melting fraction for CuO nanoparticle 5 wt. dispersed in n-octadecane PCM.

3.2. Model validation

For validation, experimental data from the study by Dhaidan et al. [35], is used. In their research, an aluminum heat sink is installed on the front wall of a CPV panel, with the bottom, top, and back walls treated as adiabatic. They studied the melting process of CuO nanoparticles dispersed in n-octadecane at a 5 wt% concentration. A comparison between the results from Dhaidan et al. [35], and the present study is shown in Fig. 4. Based on this comparison, the difference is approximately 2%, indicating that the simulation is acceptable.

To validate the numerical accuracy of the proposed model, the melting behavior of the NEPCM was compared with the available experimental data under idealized boundary condition (Fig. 4). The results showed a good agreement in terms of the melting rate and liquid fraction evolution, confirming the reliability of the numerical procedure for the phase-change modeling. However, it should be noted that this validation was only performed for a part of the model specifically the melting of the NEPCM and not for the entire CPV system. Therefore, the overall accuracy of the complete CPV model has not been directly confirmed through experimental measurements.

4. Results and Discussion

In this section, numerical results based on the governing equations of AHS and the thermophysical properties of the composite summarized in Table 5 are analyzed to investigate the thermal and electrical performance of the proposed CPV cooling system incorporating nanoparticle-reinforced phase change materials. The analyses are conducted in four consecutive sections, each focusing on a key physical aspect of the system behavior.

In the first part, the transient evolution of the liquid fraction is examined to evaluate the melting characteristics of the PCM and to assess the influence of CuO nanoparticle concentration on the phase change process. This analysis provides direct insight into the latent heat storage capability and melting rate of the NEPCM.

In the second part, the velocity magnitude within the molten PCM region is investigated to clarify the role of buoyancy-driven flow and natural convection under the Boussinesq approximation. This section highlights how nanoparticle addition affects fluid motion through simultaneous changes in thermal expansion, viscosity, and density.

In the third part, the effect of CuO nanoparticles on the average solar cell temperature (Tsc) is analyzed. This subsection directly links the thermal behavior of the PCM heat sink to the temperature regulation of the CPV cell, which is the primary objective of the cooling system.

In the fourth part, the electrical efficiency of the CPV system is evaluated as a function of the solar cell temperature. This analysis demonstrates how improvements in thermal management achieved through NEPCM and the AHS method translate into enhanced electrical performance.

4.1. Liquid fraction

Figure 5 presents the liquid fraction results for pure PCM and nanoparticle-enhanced compositions containing 3 wt% and 5 wt% CuO. A comparison of these results shows that complete melting occurs in 99 minutes for pure PCM, 95 minutes for PCM with 3 wt% CuO, and 93 minutes for PCM with 5 wt% CuO. As the nanoparticle concentration increases, the melting process accelerates due to enhanced thermal conductivity. However, exceeding the optimal nanoparticle concentration can lead to sedimentation, which diminishes the effect of buoyancy forces [38]. Additionally, an increased weight fraction of nanoparticles raises the dynamic viscosity of the mixture, which can impact the overall performance of the phase change material. Therefore, it is essential to determine and maintain the optimal nanoparticle concentration to maximize efficiency without introducing adverse effects.

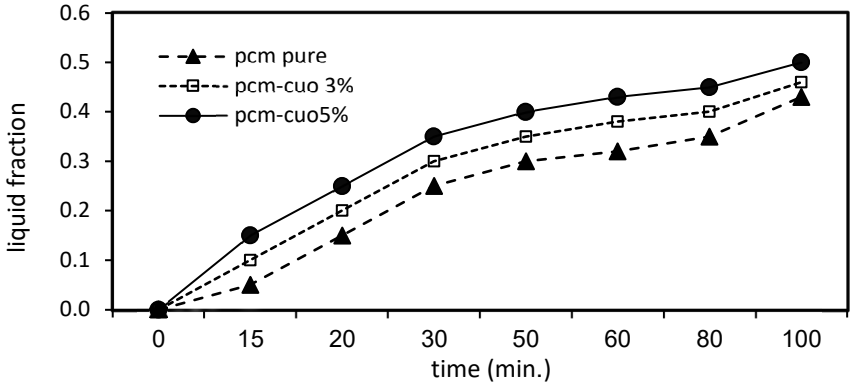

Fig. 5. Comparison of the melting processes of CuO nanoparticle dispersed in n-octadecane PCM at 5 wt% and 3 wt%, pure-PCM at complete melting.

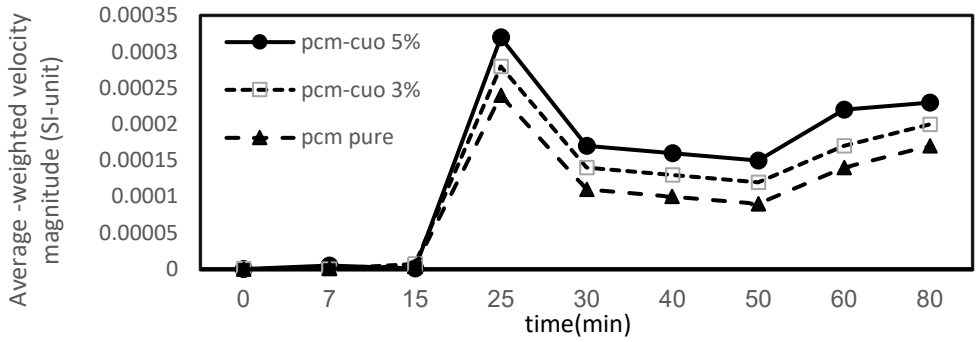

Fig. 6. Comparison average weight velocity magnitude of CuO nanoparticle enhanced in n-octadecane PCM.

4.2. Velocity magnitude

The velocity magnitude is exported from the ANSYS results based on simulated average weight velocity magnitude obtained at various time instants. These values were calculated for pure PCM as well as PCM enhanced with 3 wt% and 5 wt% CuO nanoparticles. Figure 6 indicate an overall increase in velocity for all cases, with the 5 wt% CuO composition exhibiting the highest values, followed by the 3 wt% CuO composition, and then pure PCM. This trend can be attributed to the higher thermal conductivity of the 5 wt% CuO mixture, which enhances heat transfer efficiency. As a result, the temperature gradient increases, leading to greater volumetric force differences between the solid and liquid phases of the PCM/nanoparticle composite.

4.3. Fluid heat flow analysis

4.3.1. *Analysis of heat transfer (considering the Boussinesq approximation)*

As discussed in the previous sections, the inherently low thermal conductivity of phase change materials (PCMs) limits their melting rate and overall heat transfer performance. One effective approach to mitigate this limitation is the addition of a small fraction of high-conductivity nanoparticles. In the present study, CuO nanoparticles with concentrations of 3% and 5% are employed to enhance the thermal behavior of the PCM heat sink. The temperature contour plots presented in Fig 7 illustrate the transient heat transfer characteristics for pure PCM, PCM–CuO 3%, and PCM–CuO 5% under a constant heat flux of 20 kW/m^2.

The numerical model accounts for buoyancy effects through the Boussinesq approximation, in which density variations induced by temperature differences generate gravity-driven flow within the molten PCM region. The evolution of the temperature field therefore reflects the combined contribution of conduction-dominated heat transfer at early stages and buoyancy-induced effects as melting progresses.

Pure PCM

For the pure PCM case, the temperature contours indicate a strongly conduction-dominated heat transfer mechanism throughout the process. At 20 min, thermal penetration is limited to a thin region adjacent to the heated wall, and the isotherms remain nearly straight and vertical. This behavior confirms the absence of any noticeable buoyancy-driven motion and indicates that gravity effects are negligible at this stage.

At 50 min and 80 min, the thermal front advances slowly into the domain; however, the isotherm structure remains smooth and one-dimensional. Even at the longest simulated time, heat penetration is relatively shallow, and the temperature distribution retains the characteristic profile of transient conduction from a constant-temperature boundary. This case therefore represents the lowest heat transfer rate among all studied configurations and serves as a reference baseline.

PCM–CuO 3%

When 3 wt% CuO nanoparticles are added to the PCM, a moderate enhancement in thermal performance is observed. At 20 min, the isotherms remain largely straight and confined near the heated wall, indicating that conduction still dominates the early-stage heat transfer. Compared to pure PCM, the thermal penetration depth is slightly increased due to the improved effective thermal conductivity.

At later times (50 and 80 min), the thermal front progresses further into the enclosure. Although the isotherms remain relatively smooth, minor deviations from perfect vertical alignment can be observed, suggesting the gradual influence of buoyancy forces as

melting advances. The simultaneous increase in viscosity associated with nanoparticle addition delays the development of strong natural convection, resulting in a limited but measurable heat transfer enhancement.

PCM–CuO 5%

The PCM–CuO 5 wt% configuration exhibits the most pronounced improvement in heat transfer among the investigated cases. At 20 min, heat transfer remains primarily conduction-controlled; however, slight curvature of the isotherms near the heated wall indicates the onset of buoyancy-driven flow. At 50 min and 80 min, a significantly larger portion of the enclosure becomes thermally affected compared to pure PCM and PCM–CuO 3%. The temperature contours appear more uniformly distributed, reflecting an enhanced thermal diffusion process. Despite this improvement, the flow remains relatively stable, indicating a combined conduction–buoyancy heat transfer regime rather than fully developed natural convection. The higher nanoparticle concentration effectively reduces thermal resistance and accelerates the melting process.

The comparative analysis confirms that pure PCM exhibits conduction-dominated heat transfer, while the incorporation of CuO nanoparticles improves thermal performance by increasing effective thermal conductivity and activating buoyancy effects during melting. Increasing the nanoparticle concentration from 3 wt% to 5 wt% yields the highest heat transfer enhancement and the most efficient CPV temperature regulation, which directly contributes to improved electrical efficiency. These findings are consistent with the governing equations and the Boussinesq approximation employed in the present numerical model.

4.3.2. *The impact of nanoparticles-PCM (NPCM) on CPV temperature*

One of the main objectives of analyzing CPV solar cell temperature is to determine the optimal conditions for maximizing system efficiency. Figure 8 presents the CPV temperature variations, highlighting three distinct phases:

- Section A: Heat is transferred to the CPV solar cell through conduction and then dissipated into the PCM via the aluminum wall. During this stage, the PCM-nanoparticle mixture undergoes its first phase transition, entering the mushy zone.
- Section B: This phase, known as the mushy zone, is characterized by a deceleration in temperature rise, which eventually stabilizes. This behavior is attributed to the stabilization of conductive heat transfer. At this stage, natural convection becomes the dominant mechanism, driving the phase change from a semi-solid to a fully liquid state, thereby completing the melting process.
- Section C: The temperature of the CPV solar cell continues to rise, likely due to the enhancement of natural convection, which facilitates the complete transition of the PCM into its liquid state.

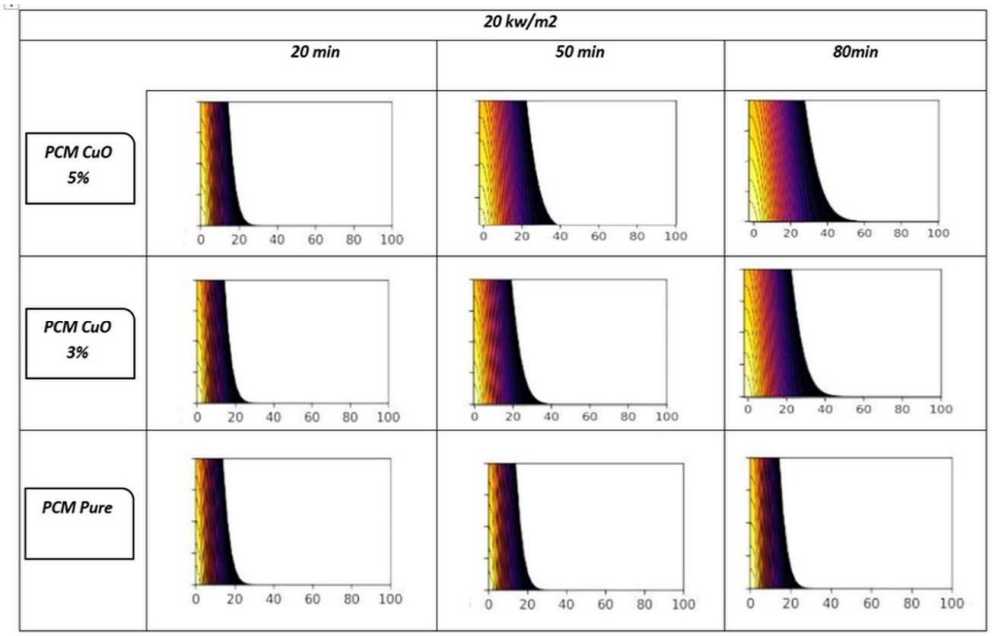

Fig. 7. Thermal contours of heat sink geometry.

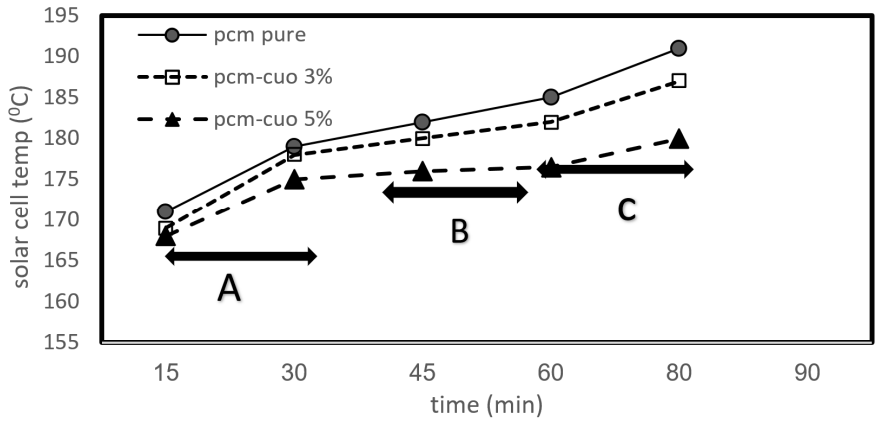

Fig. 8. Comparison of solar cell temperature of CuO nanoparticle dispersed in n-octadecane PCM at 5 wt% and 3 wt%, pure-PCM.

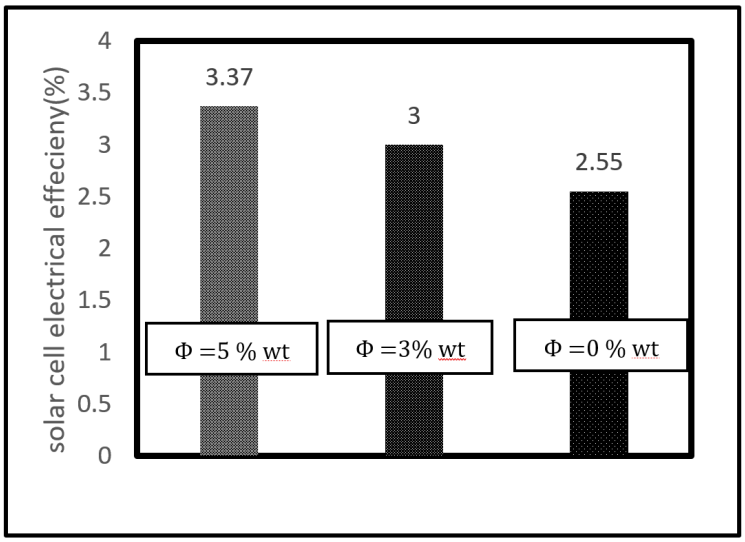

Fig. 9. Comparison of solar cell electrical efficiency: CuO nanoparticle enhanced in n-octadecane PCM at 3 wt% and 5 wt%, pure-PCM.

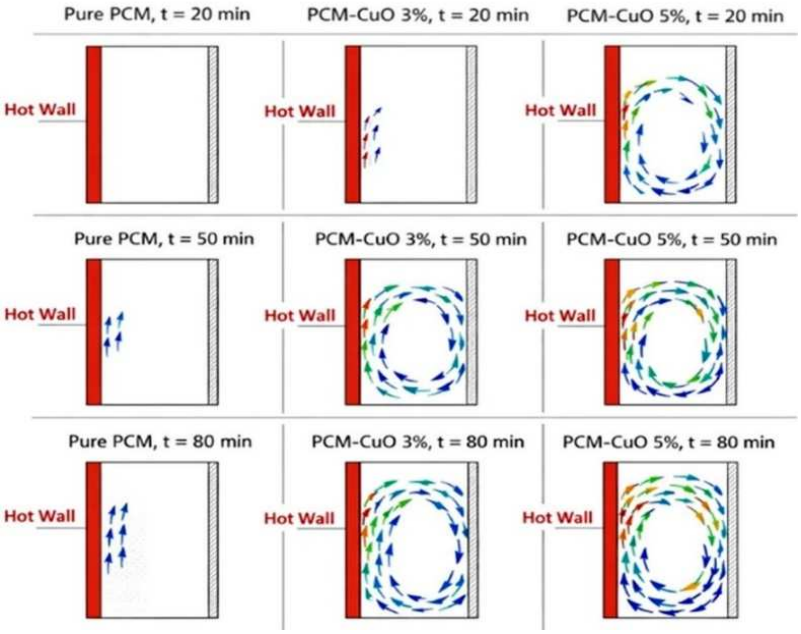

Fig. 10. Velocity vectors in the molten PCM region highlighting natural convection effects.

As shown in Fig. 8, the incorporation of nanoparticles into the PCM effectively reduces the CPV solar cell's temperature. This reduction is attributed to the increased thermal conductivity of the PCM-nanoparticle mixture, which enhances heat dissipation. At the point of complete melting, the CPV temperature for pure PCM reaches 191°C. However, with the addition of 3 wt% CuO nanoparticles, this temperature decreases to approximately 185°C, and with 5 wt% CuO, it further reduces to 180°C.

4.4. Performance of the PCM/nanoparticles CPV systems

Figure 9 compares the performance of the PCM/nanoparticle CPV system at different CuO weight fractions. The electrical efficiency of the solar cell is 3.37% for 5 wt% CuO-PCM, 3.0% for 1 wt% CuO-PCM, and 2.55% for pure PCM. These results demonstrate that incorporating CuO nanoparticles into the PCM enhances electrical efficiency, thereby improving the overall performance of the solar cell. This enhancement is primarily attributed to the increased thermal conductivity and the improved heat transfer rate of the PCM/nanoparticle composite.

5. Discussion: Benefits and Potential Limitations of Nanoparticle-Enhanced PCMs

The incorporation of nanoparticles into phase change materials (PCMs) has been widely reported as an effective approach to enhance thermal conductivity and accelerate the melting process. In the present study, the addition of CuO nanoparticles at concentrations of 3 wt% and 5 wt% significantly improves heat transfer performance, leading to faster PCM melting, lower CPV operating temperature, and enhanced electrical efficiency. However, alongside these positive effects, several potential drawbacks associated with nanoparticle-enhanced PCMs (NEPCMs) must be carefully considered to ensure realistic interpretation of the results.

One of the primary limitations of increasing nanoparticle concentration is the increase in dynamic viscosity of the molten PCM. As reported by Dhaidan et al. [35], higher nanoparticle loading increases viscous resistance, which may suppress buoyancy-driven flow and reduce the intensity of natural convection. Since natural convection plays a crucial role in enhancing heat transfer during

the melting stage, excessive viscosity can counteract the benefits of increased thermal conductivity. This trade-off explains why heat transfer enhancement does not increase linearly with nanoparticle concentration (Fig. 10).

Additionally, the increase in viscosity directly affects the Rayleigh number, leading to a reduction in buoyancy forces and weakening of convective motion within the molten PCM. As a result, heat transfer may gradually shift toward a conduction-dominated regime at higher nanoparticle concentrations, particularly in confined geometries such as PCM heat sinks.

Another important concern is the agglomeration (clustering) of nanoparticles during repeated melting–solidification cycles. Dhaidan et al. [35] emphasized that nanoparticle agglomeration may cause local non-uniformity in thermophysical properties, leading to uneven heat transfer and reduced long-term thermal performance. Closely related to this issue is sedimentation, where nanoparticles may settle under gravitational forces during the liquid phase, especially at higher concentrations. Sedimentation can significantly degrade the effective thermal conductivity and alter the melting behavior over time.

Therefore, although higher nanoparticle concentrations enhance thermal conductivity, an optimal concentration range must be identified to balance improved heat diffusion against the adverse effects of increased viscosity, weakened natural convection, agglomeration, and sedimentation. In the present study, the 5 wt% CuO case demonstrates the best overall thermal and electrical performance within the investigated range; however, further increases in nanoparticle concentration may not necessarily yield additional benefits and could even deteriorate system performance.

It should also be noted that the present numerical model assumes a homogeneous and stable suspension of nanoparticles within the PCM. Long-term degradation mechanisms such as sedimentation and agglomeration are not explicitly modeled and should be addressed in future experimental and numerical investigations.

6. Conclusion

A practical approach to enhancing the efficiency of CPV systems is the integration of a heat sink with PCM and nanoparticles. This study numerically investigated the impact of adding 3 wt% and 5 wt% CuO nanoparticles to n-octadecane PCM. The investigation focused on liquid fraction, velocity, and solar cell temperature for both PCM/nanoparticle composites and pure PCM. The results indicated that increasing the nanoparticle weight fraction improves thermal conductivity and enhances heat transfer. Specifically, compared to pure PCM, the time required for complete melting was reduced by 4 to 6 minutes, and the solar cell temperature decreased by approximately 6°C for 3 wt% CuO and 11°C for 5 wt% CuO.

Author Contributions

R. Vatandoust conducted the research, performed the analysis, and prepared the original draft of the manuscript, A. Mirabdolah Lavasani supervised the research and contributed to the conceptualization and revision of the manuscript, S. Dinarvand supervised the research, providing scientific guidance, M. Eftekhari Yazdi contributed as advisors, providing scientific guidance, M. Sardarabadi contributed as advisors, providing scientific guidance. The manuscript was written through the contribution of all authors. All authors discussed the results, reviewed, and approved the final version of the manuscript.

Acknowledgments

Not applicable.

Conflict of Interest

The authors declared no potential conflicts of interest concerning the research, authorship, and publication of this article.

Funding

The authors received no financial support for the research, authorship, and publication of this article.

Data Availability Statements

The datasets generated and analyzed during the current study are available from the corresponding author on reasonable request.

Nomenclature

A_{mush}	Mush zone constant [kg/m^3.s]	ε	Emissivity
C_p	Specific heat at constant pressure [J/kg.k]	τ	Transmissivity
CR	Concentration ratio	μ	Viscosity [Pa.s]
$G(t)$	Concentration solar irradiance [W/m^2]	σ	Stephan–Boltzmann constant
SF	Suspending fluid	ρ	Density [kg/m^3]
g	Gravitational acceleration [m/s^2]	δ	Thickness [m]
H	Total enthalpy of the material [J/kg]	η	Efficiency
$H1$	Solar cell height [mm]	λ	Liquid fraction
H	Convention heat transfer coefficient [W/m^2.k]	$\emptyset$	Eeight fraction
$h1$	Sensible enthalpy [J/kg]	**Subscripts**	
k	Thermal conductivity [W/m.K]	amb	Ambient
L	Length of the enclosure [mm]	Al	Aluminum

Lm	Latent heat [J/kg]	$conv$	Convection
m	Mass [kg]	E	EVA
$Npcm$	Nano particle - PCM	g	Glass
Q	Stored thermal energy [J/kg]	ini	Initial
$q"w$	Constant wall heat flux	l	Liquid
T	Temperature [°C]	m	Melting
t	Time [min.]	PCM	Phase change material
V	Velocity [m/s]	rad	Radiation
u, v	Velocity in x and y-axis [m/s]	$refl$	Reflected
x, y	Cartesian coordinates	ref	Reference
ΔTm	Melting temp. range	s	Solid
Greek symbols		sc	Silicon cell
α	Absorptivity	T	Tedlar
β	Solar cell temperature coefficient [1/K]	th	Thermal
$\beta 1$	Thermal expansion coefficient [1/K]	w	Wind

Reference

[1] International Energy Agency (IEA), *Technology Roadmap: Solar Photovoltaic Energy*, IEA, 2014.
[2] Natarajan, S.K., Mallick, T.K., Katz, M., Weingaertner, S., Numerical investigations of solar cell temperature for photovoltaic concentrator system with and without passive cooling arrangements, *International Journal of Thermal Sciences*, 50(12), 2011, 2514-2521.
[3] Sharma, S., Micheli, L., Chang, W., Tahir, A.A., Reddy, K.S., Mallick, T.K., Nano-enhanced phase change material for thermal management of BICPV, *Applied Energy*, 208, 2017, 719-733.
[4] Huang, M.J., Eames, P.C., Norton, B., Thermal regulation of building-integrated photovoltaics using phase change materials, *International Journal of Heat and Mass Transfer*, 47(12-13), 2004, 2715-2733.
[5] Solanki, C.S., *Solar Photovoltaics: Fundamentals, Technologies and Applications*, 3rd ed., PHI Learning, 2015.
[6] Ahmed, M., Radwan, A., Performance evaluation of new modified low-concentrator polycrystalline silicon photovoltaic/thermal systems, *Energy Conversion and Management*, 149, 2017, 593-607.
[7] Khodadadi, M., Ali Farshad, S., Ebrahimpour, Z., Sheikholeslami, M., Thermal performance of nanofluid employing NEPCM in a PVT-LFR system, *Thermal Science and Engineering Progress*, 47, 2021, 101340.
[8] Kothari, R., Kumar Sahu, S., Kundalwal, S.I., Investigation on thermal characteristics of nano-enhanced phase change material based finned and unfinned heat sinks for thermal management systems, *Chemical Engineering and Processing: Process Intensification*, 167, 2021, 108328.
[9] Aqib, M., Hussain, A., Ali, H.M., Naseer, A., Experimental case studies of the effect of Al2O3 and MWCNT nanoparticles on heating and cooling of PCM, *Case Studies in Thermal Engineering*, 18, 2020, 100-112.
[10] Zarma, I., Ahmad, M., Ookawara, S., Enhancing the performance of photovoltaic systems using nanoparticle phase change material heat sink, *Energy Conversion and Management*, 181, 2019, 559-567.
[11] Emam, M., Ahmed, M., Cooling concentrator photovoltaic systems using various configurations of phase change material heat sink, *Energy Conversion and Management*, 179, 2019, 229-242.
[12] Najafi, F., Ramezani, D., Sheykh, S., Aldaghi, A., Taheri, A., Sardarabadi, M., Passandideh-Fard, M., Experimental investigation of photovoltaic cooling using phase change materials, *Applied Thermal Engineering*, 140, 2018, 142-154.
[13] Abo-Zahhad, E.M., Haridy, S., Radwan, A., El-Sharkawy, I.I., Esmail, M.F.C., Thermal management of ultra-high concentrator photovoltaic cells: Analysing the impact of sintered porous media microchannel heat sinks, *Journal of Cleaner Production*, 180, 2018, 440-453.
[14] Radwan, A., Ookawara, S., Ahmed, M., Analysis and simulation of concentrating photovoltaic systems with a microchannel heat sink, *Solar Energy*, 126, 2016, 175-188.
[15] Radwan, A., Ahmed, M., Ookawara, S., Performance enhancement of concentrated photovoltaic systems using a microchannel heat sink with nanofluids, *Energy Conversion and Management*, 119, 2016, 43-54.
[16] Huang, M.J., Eames, P.C., Norton, B., Hewitt, N.J., Natural convection in an internally finned phase change material heat sink for the thermal management of photovoltaics, *Solar Energy Materials and Solar Cells*, 95(7), 2011, 1598-1603.
[17] Lamba, R., Montero, F.J., Rehman, T., Singh, S., Manikandan, S., PCM-based hybrid thermal management system for photovoltaic modules: A comparative analysis, *Environmental Science and Pollution Research*, 221, 2024, 122-137.
[18] Pu, J., Du, J., Zhang, B., Rong, F., Jiao, F., Hong, Y., Thermal management enhancement of photovoltaic panels using phase change material heat sinks with various T-shaped fins, *Case Studies in Thermal Engineering*, 54, 2024, 104119.
[19] Kameswara, D., Sudhakar Reddy, K., Subba Rao, Influence on solar PV performance integrated with heat sinks and nano-enhanced phase change material, *Proceedings of the Institution of Mechanical Engineers Part E: Journal of Process Mechanical Engineering*, 121, 2024, 117-125.
[20] Alipour, N., Jafari, B., Hosseinzadeh, K., Analysis of the impact of metal foam with phase change material on solar photovoltaic thermal system efficiency, *Journal of Energy Storage*, 83, 2024, 110-121.
[21] Lima-Téllez, T., Hernández-López, I., Moreno, S., Numerical study of the thermal performance of a single-channel cooling PV system using baffles and different nanofluids, *Heliyon*, 10(2), 2024, 260-278.
[22] Becheikh, N., Basem, A., Hussein, A.Z., Improving photovoltaic efficiency and financial performance through hybrid PCM cooling with nanoparticles and fins, *Case Studies in Thermal Engineering*, 55, 2024, 104132.
[23] Togun, H., Basem, A., Jweeg, M.J., Mohammed, H.I., Abed, A.M., Anqi, A.E., Development and innovation using PCM in PV cooling systems: Passive and active approaches, *Journal of Thermal Analysis and Calorimetry*, 121, 2025, 111-128.
[24] Gholami, H., Sardarabadi, M., Passandideh-Fard, M., Experimental and numerical investigation of fin-enhanced PCM heat sinks for photovoltaic thermal regulation, *Solar Energy*, 247, 2023, 361-373.
[25] Hasan, A., McCormack, A., Huang, M.J., Thermal performance of nano-enhanced phase change materials for photovoltaic cooling applications, *Applied Thermal Engineering*, 31, 2024, 1068-1075.
[26] Emam, M., Ahmed, M., Thermal management of electronic devices and concentrator photovoltaic systems using phase change material heat sinks: Experimental investigations, *Renewable Energy*, 141, 2019, 322-339
[27] Radwan, A., Ahmed, M., The influence of microchannel heat sink configuration on the performance of low-concentration photovoltaic systems, *Applied Energy*, 206, 2017, 594–611.
[28] Zhou, J., Yi, Q., Wang, Y., Ye, Z., Temperature distribution of photovoltaic modules based on finite element simulation, *Solar Energy*, 10(40), 2015, 111.
[29] Kant, K., Shukla, A., Sharma, A., Biwole, P.H., Heat transfer studies of photovoltaic panels coupled with phase change materials, *Solar Energy*, 140, 2016, 151-161.
[30] Brent, A.D., Voller, V.R., An enthalpy-porosity technique for modelling convection-diffusion phase change: Application to the melting of a pure metal, *Numerical Heat Transfer Part B*, 13(3), 1988, 297-318.

[31] Cross, M., Markatos, N.C., Voller, V.R., An enthalpy method for convection-diffusion phase change, *International Journal for Numerical Methods in Engineering*, 24(1), 1987, 271-284.
[32] Kheirabadi, A.C., Groulx, D., The effect of the mushy-zone constant on simulated phase change heat transfer, *Proceedings of the 6th International Symposium on Advanced Computational Heat Transfer*, Rutgers University, USA, 2015.
[33] Soares, N., Rosa, N., Costa, J.J., Lopes, A.G., Matias, T., Simoes, P.N., Duraes, L., Validation of different numerical models with benchmark experiments for modelling microencapsulated PCM-based applications for buildings, *International Journal of Thermal Sciences*, 159(3), 2021, 106565.
[34] Heim, D., Isothermal storage of solar energy in building construction, *Renewable Energy*, 35(4), 2010, 788-796.
[35] Dhaidan, N.S., Khodadadi, J.M., Al-Hattab, T.A., Al-Mashat, S.M., Experimental and numerical investigation of melting of phase change material/nanoparticle suspensions in a square container subjected to constant heat flux, *International Journal of Heat and Mass Transfer*, 06, 2013, 057.
[36] Brinkman, H.C., The viscosity of concentrated suspensions and solutions, *Journal of Chemical Physics*, 20(1), 1952, 571.
[37] Wakao, N., Kaguei, S., Smith, J.M., *Heat and Mass Transfer in Packed Beds*, Gordon and Breach Science Publishers, New York, 29(6), 1983, 1055.
[38] Khodadadi, M., Hosseinizadeh, S.F., Nanoparticle-enhanced phase change materials for improved thermal energy storage, *International Communications in Heat and Mass Transfer*, 34(5), 2007, 534-543.
[39] Hosseinizadeh, S.F., Khodadadi, J.M., Numerical simulation of phase change material heat sinks with nanoparticles, *International Communications in Heat and Mass Transfer*, 34(8), 2007, 1010-1017.

ORCID iD

Arash Mirabdolah Lavasani https://orcid.org/0000-0002-1770-7884
Saeed Dinarvand https://orcid.org/0000-0002-1625-8618
Mohamad Eftekhari Yazdi https://orcid.org/0000-0003-4958-1769
Mohammad Sardarabadi https://orcid.org/0000-0001-9496-6313

How to cite this article: Vatandoust R., et al., Numerical Investigation of Concentrating Photovoltaic Cooling System use a Heat Sink with Nanoparticles-Enhanced Phase Change Materials, *J. Appl. Comput. Mech.*, xx(x), 2026, 1–14. https://doi.org/10.22055/jacm.2026.48778.5490